Advances in Geo-Energy Research

Vol. 7, No. 3, p. 152-163, 2023

Original article

Research on the differential tectonic-thermal evolution of Longmaxi shale in the southern Sichuan Basin

Lei Zhao[1,2], Weijian Mao[1]*, Zongbao Liu[3], Shijun Cheng[4]

[1]*Research Center for Computational and Exploration Geophysics, State Key Laboratory of Geodesy and Earth's Dynamics, Innovation Academy for Precision Measurement Science and Technology, Chinese Academy of Sciences, Wuhan 430077, P. R. China*

[2]*University of Chinese Academy of Sciences, Beijing 100049, P. R. China*

[3]*College of Earth Sciences, Northeast Petroleum University, Daqing 163318, P. R. China*

[4]*Physical Science and Engineering, King Abdullah University of Science and Technology, Thuwal 23955-6900, Saudi Arabia*

Keywords:
Tectonic-thermal evolution
Longmaxi shale
southern Sichuan Basin
buried history
thermal evolution
hydrocarbon generation

Cited as:
Zhao, L., Mao, W., Liu, Z., Cheng, S. Research on the differential tectonic-thermal evolution of Longmaxi shale in the southern Sichuan Basin. Advances in Geo-Energy Research, 2023, 7(3): 152-163.
https://doi.org/10.46690/ager.2023.03.02

Abstract:
The southern Sichuan Basin in China holds abundant shale gas resources; however, the shale gas bearing property shows great differences due to the multiple stages of tectonic transformation. The key to revealing the shale gas differential enrichment mechanism is to explore the thermal evolution characteristics during tectonic evolution. Therefore, taking the Luzhou and Changning blocks as an example, which have obvious differences in tectonic evolution, the organic geochemical conditions of Longmaxi shale were firstly compared with the test data. Then, the thermal evolution characteristics under the background differential tectonic uplift-erosion were recovered using basin modeling techniques. The results showed that the two blocks contain similar organic geochemical conditions of the Longmaxi shale. Moreover, the hydrocarbon generation condition in Luzhou Block is greater than that in the Changning Block. Influenced by the differential tectonic evolution, the study area experienced a complex burial history and the formation of multiple unconformities. As a result, the present burial depth of Longmaxi Formation in the Luzhou Block is significantly greater than that in the Changning Block. The thermal evolution history of Longmaxi shale in the study area could be divided into three stages, including a low-temperature stage from Caledonian to Hercynian, a middle-temperature stage from Hercynian to Indosinian, and a high-temperature stage from Yanshanian to Himalayan. In addition, it was found that the Himalayan period is the main stage resulting in the differential gas bearing property of Longmaxi shale in the southern Sichuan area. Under the differential structural modification, the peak time of hydrocarbon generation in the Luzhou Block occurred earlier and the conversion rate was slightly higher than that in the Changning Block.

1. Introduction

To date, shale gas has become an important natural gas resource (Wei et al., 2022), accounting for one-fifth of the world's total output. Since the successful production of Well Wei 201 in 2010 (Shi et al., 2022a), shale gas exploration in China has been pursued for more than ten years and seen several technical breakthroughs. Shale gas production grew rapidly from 0.25×10^8 m^3 in 2012 (Qiu et al., 2020) to 220×10^8 m^3 in 2021 (Li et al., 2022a). Undoubtedly, shale gas accounts for a significant proportion of natural gas reserves and is a major contributor to the increased output in China (Xu et al., 2019). Shale gas is mainly distributed in marine basins in southern China. Sichuan Basin, especially the southern Sichuan area that is enriched in shale gas resources, has become the major focus of shale gas exploration and development in this country (Fu et al., 2019).

In order to predict the capacity of shale reservoir and explore the ability of shale to generate hydrocarbons, it is essential to clarify the effect of thermal evolution on the de-

Yandy Scientific Press

*Corresponding author.
E-mail address: zhaolei@apm.ac.cn (L. Zhao); wjmao@whigg.ac.cn (W. Mao); lzbdqpi@163.com.cn (Z. Liu); shijun.cheng@kaust.edu.sa (S. Cheng).

Received November 29, 2022; revised December 22, 2022; accepted January 6, 2023; available online January 9, 2023.

velopment of shale organic matter (Curtis et al., 2012). Unlike for conventional natural gas, organic pores can provide space for the accumulation of shale gas in addition to conventional pores (Bruns et al., 2016; Liu et and Ostadhassan, 2017). This route is comprehensively related to kerogen type and maturity (Gao et al., 2020; Li, 2021). Laboratory research has shown that the pore structure of shale changes significantly with increasing temperature, resulting in the enlargement of pore space (Chandra et al., 2021). In addition, shale samples will produce more irregular nanopores with increasing thermal maturity (Bernard et al., 2012a). Laboratory experiments on the thermal evolution of artificial shale have been used for decades to simulate the process of shale burial and hydrocarbon generation (Bowker, 2007; Hickey et al., 2007). The shale maturity and hydrocarbon generation potential can be predicted by establishing a kerogen model through experiments (Agrawal et al., 2018). Moreover, extrapolating the experimental results to the natural geological conditions can guide the exploration and development of shale gas (Bernard et al., 2012b). The thermal evolution of shale not only fundamentally affects the shale gas bearing features (Zhang et al., 2020) but also controls the evolution of reservoir pores (Klaver et al., 2016; Liu et al., 2022), thus affecting the accumulation and conservation properties (Feng et al., 2022). Therefore, shale thermal evolution has a decisive effect on the generation and accumulation of shale gas. Thus far, most researches on the shale thermal evolution process have been carried out on the shale properties alone, including kerogen structure, the total organic carbon (TOC) content estimation, vitrinite reflectance (R_o) measurement, and open system pyrolysis gas chromatography (Jarvie et al., 2007; Jenkins et al., 2008; Dembicki, 2009). Besides, research on the influence of tectonism on shale thermal evolution has been relatively weak. In addition to comprehensive geochemical information, other external factors should be considered to better characterize the thermal evolution process.

The Longmaxi (LM Fm.) shale of Luzhou (LZ) and Changning (CN) blocks in southern Sichuan have similar sedimentary characteristics but different tectonic backgrounds. Influenced by multi-stage tectonic movements in the southern Sichuan Basin, the Lower Paleozoic shale experienced significant differential uplift and erosion, which resulted in a large difference in the burial depth of organic shale layers and a complex thermal evolution process (Liu et al., 2016). Thus, studies on the thermal evolution characteristics under the differential tectonic evolution pattern can provide a scientific basis for the differential shale gas bearing properties. Meanwhile, previous studies on the LM Fm. shale in the Sichuan Basin mainly focused on its sedimentary characteristics (Zou et al., 2015; Jin et al., 2018), geochemical characteristics (Liang et al., 2014; Li et al., 2022b), and reservoir characteristics (Liu et al., 2021). It is generally agreed that the LM Fm. shale in southern Sichuan has favorable conditions for shale gas occurrence, such as wide area, large thickness of shale concentration section that is rich in organic matter, high content of organic matter, and optimal rock brittleness. Moreover, the shale stratum has experienced complex tectonic movements and a high degree of thermal evolution. Meanwhile, there is a lack of comparison between the tectonic evolution of different blocks, and studies on the influence of differential tectonic evolution on the shale thermal evolution history and hydrocarbon generation history have been scarce. Thus, based upon measured R_o values, this paper recovered the thermal evolution history of the LM Fm. shale using basin simulation techniques considering the background of structural differences in the southern Sichuan area.

2. Geological background

The Sichuan Basin is a superimposed basin developed on the Yangtze craton located in Southwest China (Shi et al., 2021), with an exploration area of 18.1×10^4 km^2 (Jin et al., 2018). It generally presents a NE-trending distribution (Shi et al., 2022b), surrounded by four fold belts of the Qiyueshan in the east, Longmenshan in the west, Meishan-Wushan in the southern and Micangshan-Dabashan in the north (Guo et al., 2020). The six second-order tectonic units are shown in Fig. 1. The study area is located in the southern Zone.

Strata of the Paleozoic and Mesozoic were successively deposited on the Sinian Yangtze basement in the Sichuan Basin. However, several strata are missing due to the multiple stages of tectonic movements, as shown in Fig. 2 (Liu et al., 2021). After the deposition of Cambrian, Ordovician (O) and Silurian (S) in the Paleozoic, the study area entered differential tectonic evolution stages. The Caledonian movement resulted in the disappearance of Devonian (D) and most Carboniferous (C) systems, and only a thin set of C_1 remained (Jin et al., 2018). Deposition at the top of Lower Permian (P_1) stopped due to Hercynian movement (Yang et al., 2016). Therefore, three tectonic evolution stages can be specified: the early craton depression stage from the late Sinian to the middle Triassic, the foreland basin stage from the late Triassic to the late Cretaceous, and the uplift-erosion stage since the Paleogene (Chen et al., 2017; Liu et al., 2021). During the O_3 to S_1 period, the Sichuan Basin was in a clastic-shelf sedimentary environment. However, due to the Caledonian Movement, the southern and northeastern parts were in deep-water continental shelf facies. Under the anoxic environment with lower water energy, huge thick organic shale formed (Tang et al., 2020). The LM Fm. shale in the east is thicker than in the west, with a maximum thickness reaching 400-600 m. In addition, LZ Block is distributed in the deposition center of the LM Fm. with a thickness ranging from 500 to 600 m. Meanwhile, the thickness is between 200 and 400 m in the CN Block (Fig. 1). Apart from the obvious variations in thickness, the burial depths of the LM shale in the two blocks are also different. The maximum buried depth difference is up to 2,000 m, indicating that there must be differences in uplift and erosion between them.

The lower LM Fm. in the study area mainly consists of dark gray-black sandy, carbonaceous and graptolite shales interbedded with bioclastic limestone, while the upper part presents gray-yellow-green shales, sandy shales, with siltstone and marl interlayers (Fig. 2).

Due to the characteristics of in-source accumulation and in-situ accumulation of shale gas (Zhao et al., 2021), it is important to clarify the distribution of source rocks to explore

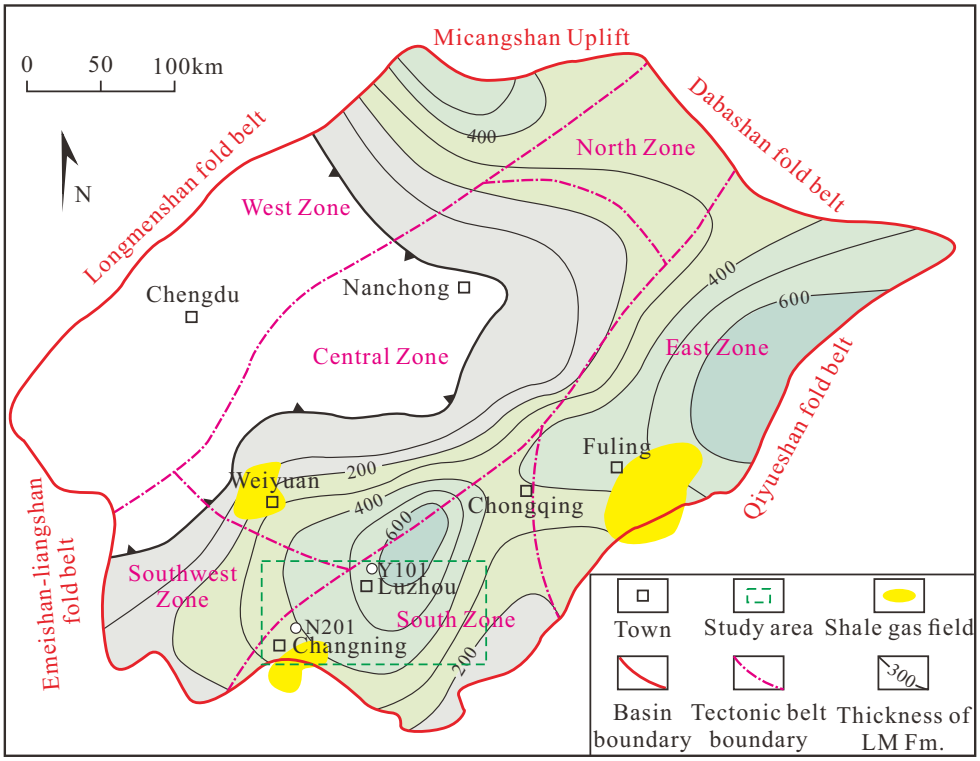

Fig. 1. Location of the study area (modified from Tang et al. (2020)).

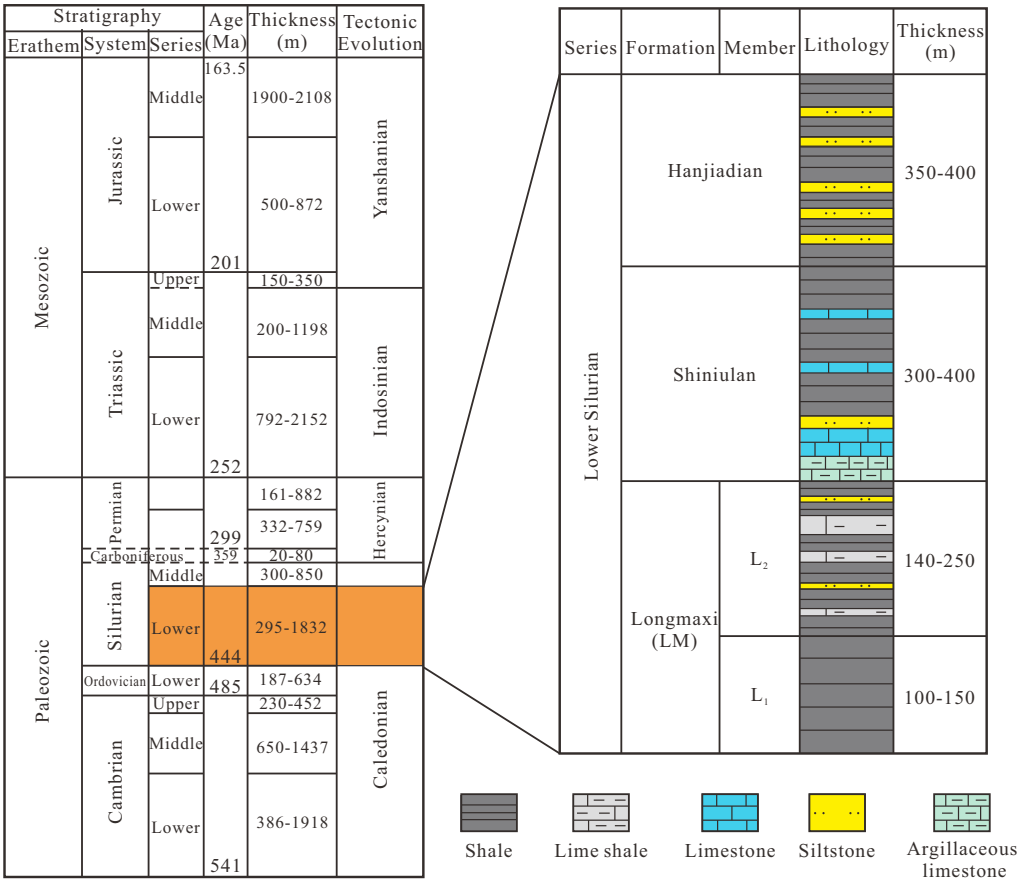

Fig. 2. Stratigraphic diagram of the study area (the left is from Liu et al. (2021) and the right is from Shi et al. (2022b)).

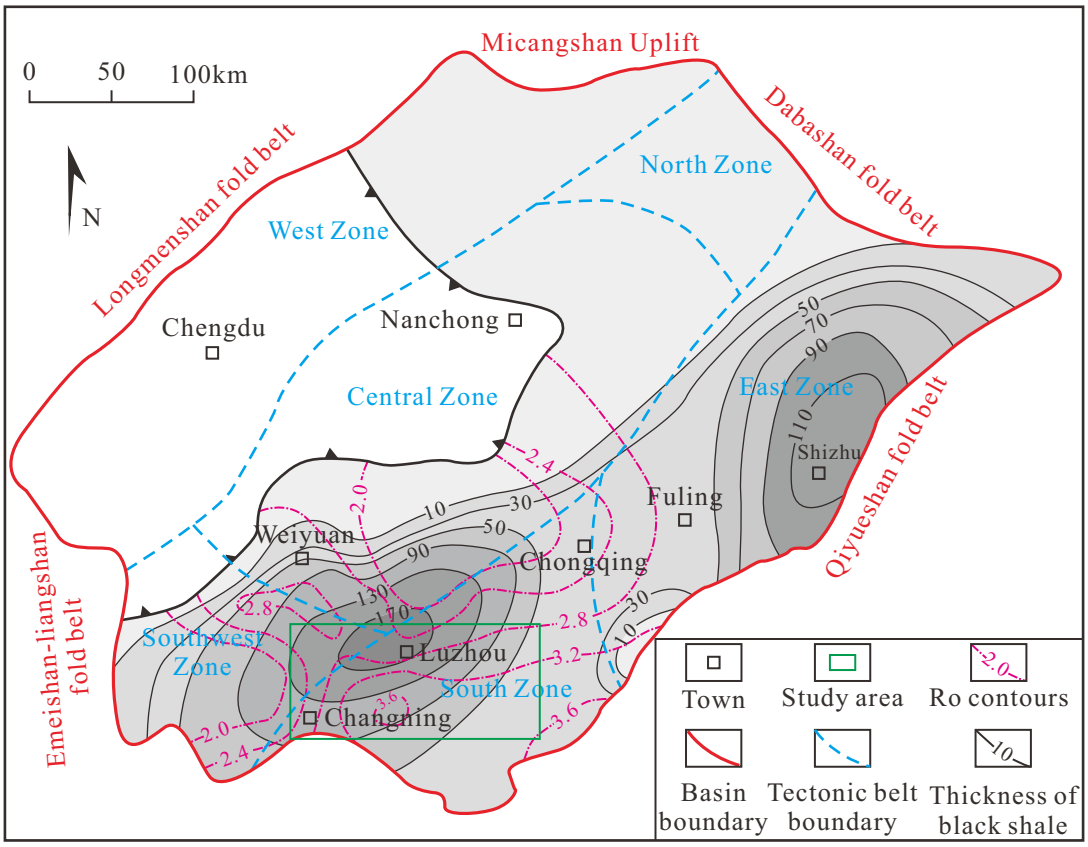

Fig. 3. Distribution of effective source rocks in the LM Fm. shale (modified from Dai et al. (2014) and Zou et al. (2015)).

the thermal evolution history of the LM Fm. shale in depth. Past research has proved that the sedimentary environment of the LM Fm. insouthern Sichuan is mainly composed of calcareous semi-deep-water and deep-water shelf facies (Zou et al., 2015). Many LM Fm. shales can be found across the research area, and their thickness is generally 50-600 m (Fig. 1). Among them, shales rich in organic matter (TOC>1%) are usually found in the lower part of the LM Fm., and their thickness is generally 30-170 m. It gradually thins to the northwest, and there are two thickness centers in the Luzhou and Shizhu regions (Fig. 3). Across the research area, the shale rich in organic matter in the LZ Block is relatively thick, generally exceeding 100 m, while that in the CN Block is relatively thin, ranging from 30 to 50 m.

3. Samples and methods

A total of 30 shale sample cores were collected from the LZ and CN blocks in southern Sichuan. The depth of samples from the LZ Block was between 3,490 to 4,230 m, and it was between 2,100 to 2,570 m in the CN Block. The samples were all black shale.

In order to clarify the organic geochemical conditions and thermal evolution characteristics of LM Fm. shale in the southern Sichuan area, this paper carried out a R_o test and rock pyrolysis experiment on the above 30 samples, and tested the macerals and carbon isotopes of kerogen on 12 samples.

The R_o test was carried out using a DM4500P polarizing microscope (Choudhury et al., 2022). After the shale sample was crushed into 100 mesh powder, ROCK Eval 7 was utilized to test the rock pyrolysis characteristics according to the National Standard of "Rock pyrolysis analysis" (GB/T 18602-2012). The parameters obtained in the experiment included gaseous hydrocarbon content (S_0), free hydrocarbon content (S_1), kerogen hydrocarbon content (S_2), dead carbon content (S_4), and maximum pyrolysis peak temperature (T_{max}). It should be noted that TOC was calculated by the following formulas:

$$\mathrm{TOC} = \mathrm{PC} + \mathrm{RC} \quad (1)$$

$$\mathrm{PC} = 0.083 \times (S_0 + S_1 + S_2) \quad (2)$$

$$\mathrm{RC} = S_4/10 \quad (3)$$

where PC represents the effective carbon content and RC represents the residual carbon content (Peters et al., 2016; Hazra et al., 2017).

In addition, two key Wells (Y101 and N201) in the LZ and CN blocks were selected to numerically simulate the burial history affected by differential structural evolution using PetroMod Software. The required parameters included the depth and deposition age of layers, eroded age, eroded depth, and lithology (Makeen et al., 2016), and the thermal evolution history could be numerically simulated using the boundary condition data, such as paleo-temperature, paleo-water depth, and paleo-heat flow (Zhu et al., 2009), as shown in Tables 1 and 2. The simulation results were corrected using the

Table 1. Numerical simulation parameters of shale burial history in the CN Block.

Layer	Deposition age (Ma)		Eroded age (Ma)		Depth (m)		Thickness (m)	Eroded depth (m)	Lithology	HF (mW/m^2)
	From	To	From	To	Top	Base				
Q	4	0	96	4	0	12	12	5600	Clay & Sands	48
K	133	96	-	-	12	12	0	-	Sands	50
J	210	133	227	210	12	12	0	360	Sands	52
T	251	227	264	251	12	850	838	180	Sands	53
P	295	264	399	295	850	1560	710	550	Limestone	67
S	439	399	-	-	1560	2510	950	-	Shale	52

Table 2. Numerical simulation parameters of shale burial history in the LZ Block.

Layer	Deposition age (Ma)		Eroded age (Ma)		Depth (m)		Thickness (m)	Eroded depth (m)	Lithology	HF (mW/m^2)
	From	To	From	To	Top	Base				
Q	4	0	96	4	0	11	11	1200	Clay	48
K	133	96	-	-	11	1457	1446	-	Sands	50
J	210	133	227	210	1457	2348	891	815	Sands	52
T	251	227	264	251	2348	3239	891	645	Sands	53
P	295	264	399	295	3239	3517	278	510	Limestone	67
S	439	399	-	-	3517	4612	1095	-	Shale	52

measured R_o values.

Seven steps were followed in this research: clarify the geological features of LM Fm. shale, contrastive study of the geochemical characteristics, clarification of the differences in the hydrocarbon generation characteristics of LM Fm. shale in the two blocks, restoration of the burial history of typical wells, restoration of the thermal history of LM Fm. shale, restoration of the hydrocarbon generation history of LM Fm. shale, and clarification of the effect of differential tectonic uplift on the thermal evolution of LM Fm. (Fig. 4).

4. Results

4.1 Organic matter abundance

Several methods can be used to assess the organic matter abundance (OMA in short) in source rocks, including measuring TOC, the potential of hydrocarbon generation ($S_1 \times S_2$), asphalt chloroform "A", etc. (Peng et al., 2016). However, the OMA measured in laboratory experiments only represents the residual OMA after hydrocarbon generation, which usually cannot reflect the true OMA. Past research has proved that the residual TOC had a good linear positive correlation with the original TOC (Jarvie et al., 2007). Therefore, for source rocks with high maturation, the measured TOC can also directly reflect the OMA, and TOC>1.0% is regarded as the key condition for a high production of shale gas (Romero-Sarmiento et al., 2013). Therefore, TOC was used in this paper to evaluate the OMA in the LM Fm. shale.

Table 3 shows 16 experimental results of 30 samples. It can be seen that the TOC of the LM Fm. shale is retained between 0.16 and 6.33%, and the mean value is 2.96%. In addition, the TOC of 83% of samples is greater than 1%, that of 63% of samples is greater than 2%, and that of 46% of samples is greater than 3% (Fig. 5(a)). These data can provide a solid foundation for formatting large-scale shale gas reservoirs at the LM Fm. in southern Sichuan. Moreover, the TOC in the LZ Block is significantly larger than that in the CN Block (Fig. 5(b)). The TOC in the LZ Block is generally more than 2% with an average of 3.92%, and it is greater than 3% for more than 80% of samples. However, the TOC at the CN Block is retained between 0.16% and 3.61% with a mean value of 1.99%, and it is less than 2% for more than 60% of samples. In addition, as the depth increases, the TOC shows an obvious growth trend (Fig. 6). TOC is related to the hydrocarbon generation and expulsion efficiency of source rocks (Bitchong et al., 2022); however, these are often very low under natural conditions. In this case, the TOC will not decrease with increasing depth (or degree of evolution).

4.2 Types of organic matter

The ratio of C, H, O atoms is generally used to determine the type of organic matter. However, thermal maturation has a large effect on the atomic components of kerogen (Nie et al., 2020; He et al., 2022). The maceral compositions can reflect the pattern of organic matter and further determine the kerogen type. The carbon isotope composition of kerogen (δ^3C_{org}) reflects its biological precursors, which will not change significantly after diagenesis and thermal maturation.

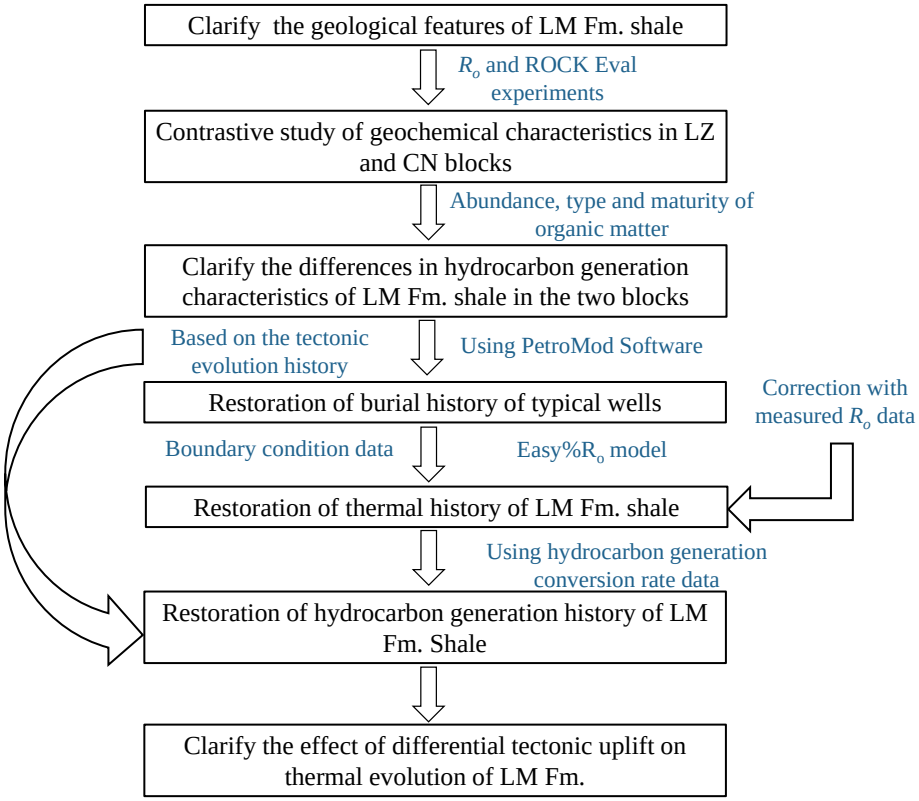

Fig. 4. Diagram showing the workflow.

Table 3. Experimental results of shale pyrolysis of the LM Fm. shale.

No.	Depth (m)	TOC (%)	S_0 (mg/g rock)	S_1 (mg/g rock)	S_2 (mg/g rock)	T_{max} (°C)	PI	HI (mg/g TOC)
CN-001	2100.65	0.16	0.001	0.122	0.148	478	0.451	95.355
CN-003	2208.15	0.35	0.003	0.122	0.241	482	0.336	68.743
CN-005	2269.90	1.14	0.001	0.011	0.029	468	0.278	2.553
CN-007	2293.10	1.06	0.002	0.010	0.025	563	0.289	2.340
CN-009	2329.30	1.23	0.002	0.011	0.031	551	0.255	2.498
CN-011	2362.45	1.51	0.001	0.009	0.025	551	0.265	1.681
CN-013	2490.50	1.15	0.000	2.118	2.317	444	0.478	201.461
CN-015	2567.80	3.57	0.001	0.014	0.039	551	0.262	1.087
LZ-001	3495.90	2.45	0.000	0.020	0.030	451	0.400	1.227
LZ-003	3514.15	1.49	0.000	0.020	0.040	449	0.333	2.685
LZ-005	3525.30	4.51	0.000	0.020	0.040	466	0.333	0.888
LZ-007	3527.55	5.35	0.000	0.020	0.030	474	0.400	0.561
LZ-009	3534.75	5.17	0.000	0.020	0.040	488	0.333	0.774
LZ-011	3544.65	3.79	0.000	0.010	0.030	465	0.250	0.793
LZ-013	3795.60	3.90	0.000	0.020	0.040	476	0.333	1.027
LZ-015	4289.30	6.33	0.000	0.010	0.040	537	0.200	0.632

Notes: PI denotes the production index that is equal to $S_1/(S_1+S_2)$, HI is the hydrogen index that is equal to $(S_2 \times 100/\text{TOC})$.

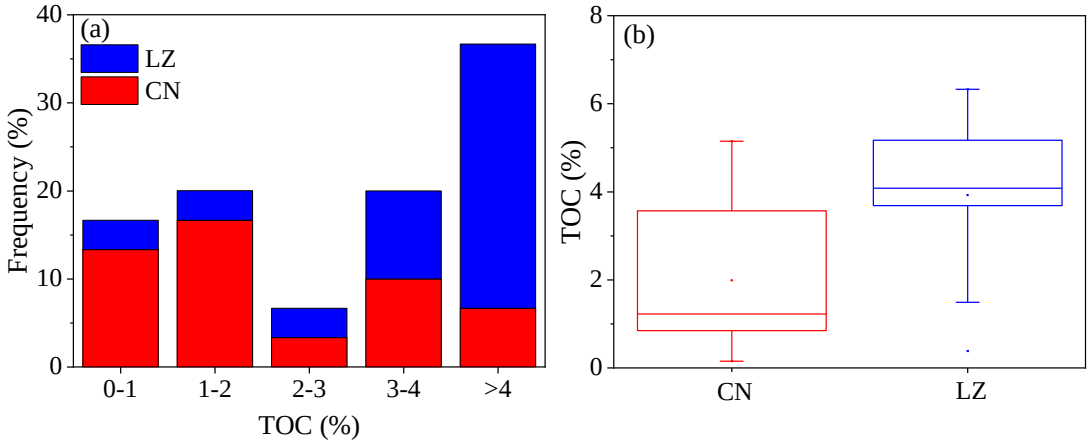

Fig. 5. (a) TOC distribution frequency and (b) box pattern of the LM Fm. shale.

Table 4. Maceral compositions and carbon isotopes of kerogen from the LM Fm. shale.

No.	Depth (m)	δ^3C_{org} (‰)	Saprolite (%)	Vitrinite (%)	Exinite (%)	Inertinite (%)	TI
CN-004	2243.55	-30.50	82.76	0.00	17.15	0.09	91.25
CN-006	2291.75	-29.90	72.85	5.12	21.89	0.14	79.82
CN-008	2311.95	-30.40	81.84	2.17	15.79	0.20	87.91
CN-010	2344.00	-30.80	85.68	3.95	10.23	0.14	87.69
CN-012	2380.70	-28.30	76.75	12.78	10.17	0.30	71.95
CN-014	2495.85	-30.40	84.89	1.56	6.98	6.57	80.64
LZ-005	3525.30	-28.60	74.56	11.32	14.08	0.04	73.07
LZ-007	3527.55	-29.20	80.08	7.89	11.85	0.18	79.91
LZ-009	3534.75	-30.50	83.15	4.28	12.43	0.14	86.02
LZ-011	3544.65	-29.80	75.88	8.21	15.89	0.02	77.65
LZ-013	3795.60	-31.00	84.78	1.28	13.81	0.13	90.60
LZ-015	4289.30	-30.80	85.68	0.95	7.19	6.18	82.38

Notes: TI=(100×Saprolite+50×Exinite-75×Vitrinite-100×Inertinite)/100.

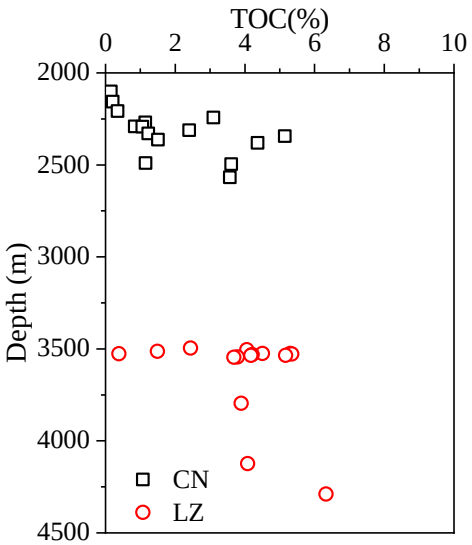

Fig. 6. Scatter plot of TOC variation with depth in the LM Fm. shale.

Therefore, the organic matter type was systematically studied using the dominant compositions and the carbon isotope composition of kerogen.

As shown in Table 4, the LM Fm. shale is dominated by saprolite with a mean value of 80.74%. The next component is exinite with a mean value of 13.12%, while the proportions of vitrinite and inertinite are relatively low. The type index (TI) of the LM Fm. shale is between 71.95 and 91.25, with a mean value of 82.41. Moreover, the carbon isotopes of kerogen are generally light, and δ^3C_{org} ranges from -31.00‰ to -28.30‰, with an average of -30.02‰. Therefore, they were considered as kerogen types I and II_1.

4.3 Maturity of organic matter

Shale maturity can be analyzed using the R_o and the maximum temperature of pyrolysis (T_{max}) (Shalaby et al., 2011). As shown in Fig. 7, the R_o of the LM Fm. shale is generally above 2.0% with an average of 2.4% and its T_{max}

is greater than 440 °C, indicating that the LM Fm. shale is in high- to over-mature state.

4.4 Burial history of the LM Fm. shale

As mentioned above, the southern Sichuan area generally experienced complex tectonic movement, causing stratum uplift and erosion. Several unconformities exist between S and P, between P_1 and P_3, between T and J, and between Cz and Mesozoic. Zhu et al. (2009) restored the amount of denudation in each denudation period.

The thickness of S sediments could reach more than 1,600 m under the differential tectonic evolution pattern in the study area. However, the Caledonian Movement during the late S_2 to C_2 caused the erosion of S_3, and the erosion thickness was about 500 m. During this period, the LM Fm. was shallowly buried. Subsequently, during the Hercynian Movement, the strata continued to rise and denudate, especially from the late P_2 to the early P_3. The strata in the LZ Block eroded by 645 m and the CN Block by 180 m. The buried depth of the LM Fm. in this period is about 2,000 m in the CN Block and 2,100 m in the LZ Block. After the Indosinian period started, deep deposition occurred continuously in the southern Sichuan area. By the end of T_2, the buried depth of the LM Fm. was 3,650 m in the CN Block and 3,050 m in the LZ block. Later, the crust rose again, resulting in 815 m denudation in the LZ Block and 360 m in the CN Block. In the Yanshanian period, extensive sedimentation began to occur in the southern of Sichuan, and the buried depth of the LM Fm. exceeded 6,000 m. From the Late Cretaceous to the present, the southern Sichuan area entered the Himalayan Movement period, and 5,600 m strata were eroded in the CN Block and 1,200 m in the LZ Block. Under the influence of differential uplift and erosion, the current burial depth of the LM Fm. is about 2,510 m in the CN Block and about 4,612 m in the LZ Block (Tables 1 and 2).

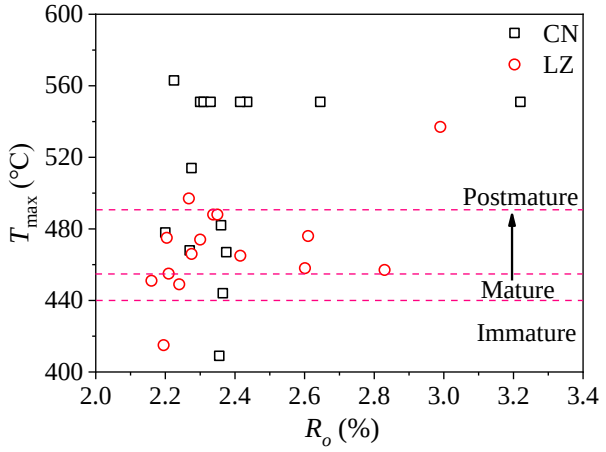

Fig. 7. Intersection diagram of R_o and T_{max} of the LM Fm. shale.

5. Discussion

5.1 Thermal evolution history

As shown in Figs. 8 and 9., there is a good direct matching relationship between the simulation results and the measured values.

The thermal evolution history controls the hydrocarbon generation process. According to the temperature variation characteristics at the bottom of the LM Fm. and the conditions of differential structural uplift and erosion, the thermal evolution process of the LM Fm. shale is composed of the following three stages:

Stage 1 (-399 Ma ago): This is the sedimentary stage of the LM Fm. when the formation temperature increased gradually with the rise of burial depth. By the late Early Devonian, the temperature of LM Fm. in the CN and LZ blocks was 93.6 °C and 100 °C, respectively. Later, the crust was raised owing to the Caledonian Movement, which resulted in the depth of LM Fm. gradually becoming shallower and the temperature

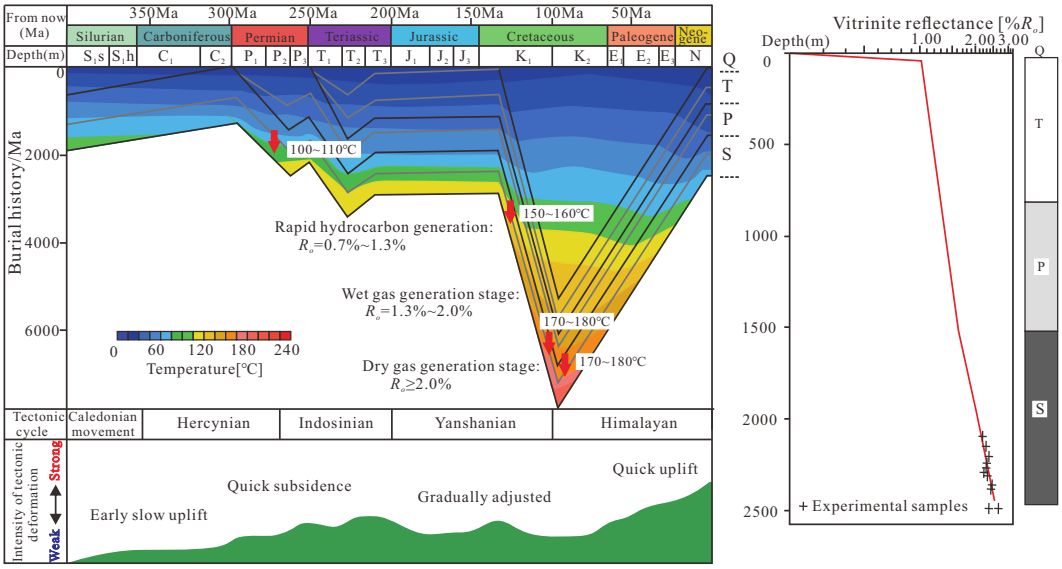

Fig. 8. Burial history curve of "burial-hydrocarbon generation-uplift-erosion" and the paleo-temperature zone in the CN Block.

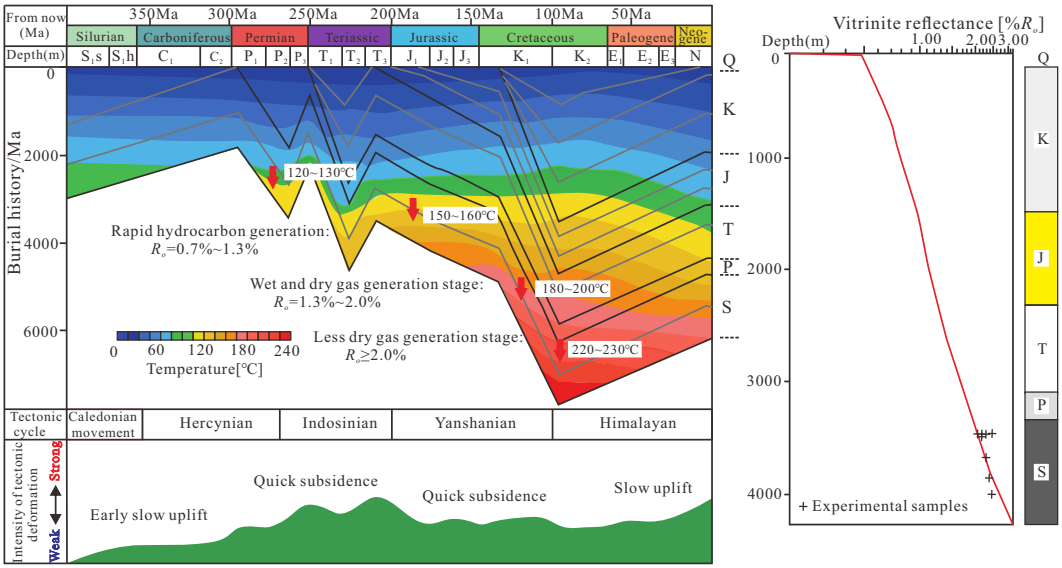

Fig. 9. Burial history curve of "burial-hydrocarbon generation-uplift-erosion" and paleo-temperature zone in the LZ Block

decreasing. Until the late Carboniferous (295 Ma ago), the temperature of the CN and LZ blocks decreased to 64 °C and 67 °C, respectively.

Stage 2 (at 295-251 Ma): At this stage, the LM Fm. was buried deep again to receive deposition, and the depth of strata gradually increased. Until the end of the Middle Permian (264 Ma ago), the temperature in the CN and LZ blocks reached 105.8 °C and 125.5 °C, respectively. Later, the crust was raised again controlled by the Hercynian Movement, the buried depth of the LM Fm. became shallower, and the temperature decreased. Up to the early Triassic (251 Ma ago), the formation temperature of the CN and LZ blocks was about 94 °C and 82 °C, respectively.

Stage 3 (at 250 Ma-present): After the end of the Hercynian Movement, the strata were buried deep again to receive deposition, and the buried depth of the LM Fm. increased rapidly. At this time, the depth of the 96 Ma strata reached its maximum. The formation temperature of the CN and LZ blocks was as high as 198.6° and 232°, respectively. Later, under the influence of the Himalayan Movement, the Earth's crust rose again, the buried depth of LM Fm. became shallower, and the temperature decreased. The present formation temperature of the CN and LZ blocks is 71° and 167°, respectively.

The LM Fm. in southern Sichuan shows a similar "burial-hydrocarbon generation-uplift-erosion" evolution pattern. From the Indosinian period, the LM Fm. shale in the LZ Block experienced a step-type formation temperature change, namely, "slow cooling (Hercynian)-fast warming (Indosinian and Yanshanian)-slow cooling (Himalayan)" under the influence of differential tectonic uplifting and denudation. In contrast, the LM Fm. shale in the CN Block presents a steep temperature change, namely, "slow cooling (Hercynian)-rapid warming (Indosinian and Yanshanian)-rapid cooling (Himalayan)". There is an inconsistency in the formation temperature change in the study area, which is caused by differential structural modification. The dissimilar tectonic evolution in the Himalayan period is an important reason for the difference in the gas bearing and measurement conditions of LM Fm. in the study area.

5.2 History and potential of hydrocarbon generation

It can be seen from Table 3 that the TOC of the LM Fm. shale is very high, which provides the material foundation for generating a large amount of natural gas. However, the contents of S_1 and S_2 are very low, that is, generally less than 0.1 mg/g rock. The calculated HI is generally less than 10 mg HC/g TOC, which means that the residual potential for generating hydrocarbon is insufficient, mainly due to the high maturity. Moreover, the intersection diagram of T_{max} and PI can also be used to determine the material source of hydrocarbons (Shalaby et al., 2011). As shown in Fig. 10, the LM Fm. shale in the research region has high maturity, and the oil and gas are all generated in situ or from internal carbon.

The R_o evolution history was recovered using the Sweeney and Burnham (1990) _Easy%R_o model on the basis of temperature evolution. Furthermore, the hydrocarbon generation evolution process was simulated according to the TI kerogen hydrocarbon generation kinetic model proposed by Behar et al. (1997), which can be described by the hydrocarbon generation transportation rate (TR). The evolution histories of maturation and hydrocarbon generation for the LM Fm. shale in the CN and LZ blocks are shown in Fig. 11.

Before 399 Ma, the R_o of LM Fm. shale in the CN Block was less than 0.5%, which was in the immature stage and had not reached the hydrocarbon generation threshold. From 399 to 270 Ma ago, the R_o of the LM Fm. shale was between 0.5% and 0.7%, indicating that the mature stage and shale had reached the hydrocarbon generation threshold. However, the thermal maturation at this stage was low, and the TR was less than 0.1%. From 270 to 122 Ma ago, the LM Fm. shale began to rapidly generate hydrocarbon, with R_o between 0.7%

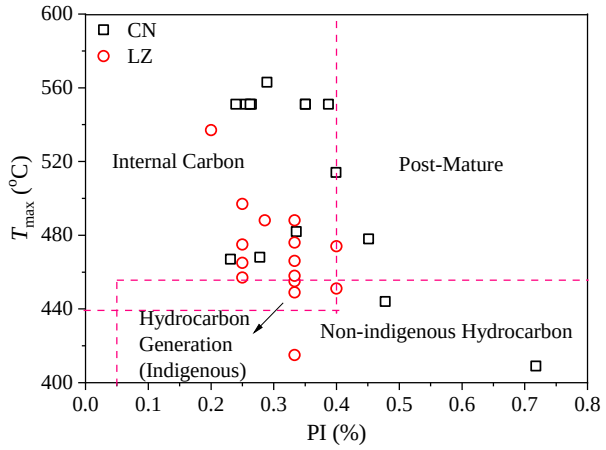

Fig. 10. Intersection diagram of the PI and T_{max} of LM Fm. shale.

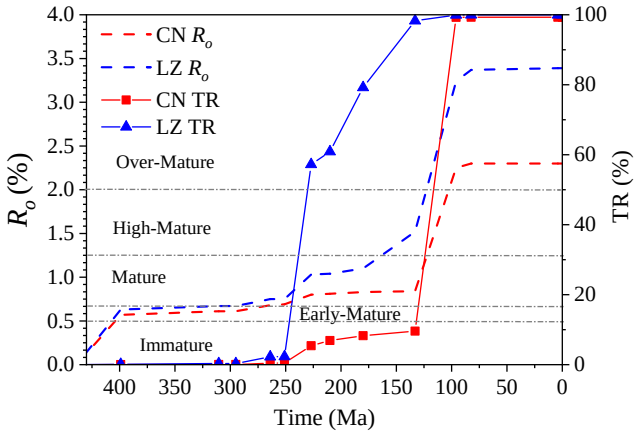

Fig. 11. Evolutionary history of R_o and TR in the LM Fm. shale.

and 1.3%. The tectonic activity of "strong at the beginning and weak at the end" made the strata temperature of shale buried under high pressure gradually increase from 100-110 to 150-160 °C. At this stage, the conversion rate of hydrocarbon generation increased rapidly to about 30%. From 122 to 103 Ma ago, the LM Fm. shale produced a large amount of wet gas, and its R_o was between 1.3% and 2.0%, which corresponds to the high maturity stage. Due to the high pressure and rapid burial process, the formation temperature gradually increased from 150-160 to 170-180 °C, and the hydrocarbon generation conversion rate continued to increase to 50% at this stage. From 103 to 96 Ma ago, the tectonic activity in this area was weak, and the thermal evolution of the LM Fm. shale increased further. When the R_o is greater than 2.0%, the source rock is overly mature, and can generate a large amount of dry gas. Hydrocarbon generation was basically completed at this stage, and the TR was as high as 99.3% (Fig. 11).

The hydrocarbon generation history of the LZ Block is different from the CN Blocks. Before 407 Ma ago, the R_o of LM Fm. shale in the LZ Block was less than 0.5%, which was in the immature stage and had not entered the threshold of hydrocarbon generation. From 407 to 280 Ma ago, the R_o of LM Fm. shale was between 0.5% to 0.7%, and the shale began to enter the threshold of hydrocarbon generation. This was slightly earlier than that for the CN Block, but the thermal maturation at this stage was low, the amount of hydrocarbon generation was small, and the highest hydrocarbon generation conversion rate was 0.33%. 280-186 Ma ago, the shale of the LM Fm. began to generate hydrocarbon rapidly, and the R_o of the formation was between 0.7% to 1.3%. At this time, the LM Fm. shale was buried under high pressure, and the formation temperature gradually increased from 120-30 to 150-160 °C. During this period, the conversion rate of hydrocarbon generation increased rapidly to about 70%. 186-122 Ma ago, the tectonic strength was weak. The R_o of the LM Fm. was between 1.3% and 2.0%, indicating the high maturity of the LM Fm. shale. During the period of 122-96 Ma, the thermal maturation of LM Fm. shale increased further, with R_o greater than 2.0% and over maturation. In this period, the formation temperature was 220-230 °C and the TR was 99.97% (Fig. 11).

The two blocks have experienced similar but not identical hydrocarbon generation histories due to their different tectonic evolution. In the LZ Block, the hydrocarbon generation peaked earlier and the TR was slightly higher compared with the CN Block (Fig. 11). That is, structural differences and tectonic activities led to differences in the hydrocarbon generation potential in different periods. However, the way differential tectonic activity affects the thermal evolution of organic shale needs more in-depth study. Also, performing quantitative research on the thermal evolution characteristics of organic shale under differential tectonic activity is the next important task.

6. Conclusions

The tectonic evolution of LZ and CN blocks obviously differs, which can be used to analyze the differential tectonic-thermal evolution of LM Fm. shale. In this paper, the organic geochemical conditions of LM Fm. shale were firstly compared using geochemical test data. Next, the thermal evolution history under the background differential tectonic uplift-erosion was recovered using basin modeling techniques. The results are listed as follows:

1) The LM Fm. shale in the southern Sichuan area has optimal shale gas generation conditions, featured by great thickness, high abundance of organic matter, oil-generating kerogen and high- to over-maturation. These conditions are better in the LZ Block than in the CN Block. Influenced by differential structural uplift and erosion, the study area presents a complex burial history and multiple unconformities. As a result, the present burial depth of LM Fm. in the LZ Block is significantly deeper than that in the CN Block.
2) In the context of differential tectonic evolution, the LM Fm. shale in southern Sichuan has experienced a pattern of "burial, hydrocarbon generation, uplift, and erosion", which includes three stages: a low-temperature stage from the Caledonian to the Hercynian, a middle-temperature stage from the Hercynian to the Indosinian, and a high-temperature stage from the Yanshanian to the Himalayan.

Among them, Himalayan is the main period for differential tectonic uplift and erosion, leading to the differential gas bearing in the LM Fm. shale in the study area.

3) The hydrocarbon generation process of the LM Fm. shale is composed of five stages of non-hydrocarbon generation, little hydrocarbon generation, rapid hydrocarbon generation, massive hydrocarbon generation, and stagnation hydrocarbon generation. The final TR is nearly 100%, indicating that the remaining potential is insufficient. Under the differential structural modification, the hydrocarbon generation in the LZ Block peaked earlier and TR was slightly higher compared with the CN Block.

Acknowledgements

This work was supported by the National Science Foundation of China (Nos. 42130808, 41974163 and 42172161).

Conflict of interest

The authors declare no competing interest.

References

Agrawal, V., Sharma, S. Molecular characterization of kerogen and its implications for determining hydrocarbon potential, organic matter sources and thermal maturity in Marcellus Shale. Fuel, 2018, 228: 429-437.

Bernard, S., Horsfield, B., Schulz, H. M., et al. Geochemical evolution of organic-rich shales with increasing maturity: A STXM and TEM study of the Posidonia Shale (Lower Toarcian, northern Germany). Marine and Petroleum Geology, 2012a, 31(1): 70-89.

Bernard, S., Wirth, R., Schreiber, A., et al. Formation of nanoporous pyrobitumen residues during maturation of the Barnett Shale (Fort Worth Basin). International Journal of Coal Geology, 2012b, 103: 3-11.

Bitchong, A. M., Ottou, J. P. B., Bitjong, S. A., et al. Preliminary source rock evaluation, paleo-depositional environment and hydrocarbon generation potential of the cretaceous organic-rich outcrops of Mayo-Figuil River, Babouri-Figuil Basin, Northern Benue Trough (Yola arm) Cameroon: Insights from bulk geochemistry. Journal of African Earth Sciences, 2022, 192: 104568.

Bowker, K. A. Barnett shale gas production, Fort Worth Basin: Issues and discussion. AAPG Bulletin, 2007, 91(4): 523-533.

Bruns, B., Littke, R., Gasparik, M., et al. Thermal evolution and shale gas potential estimation of the Wealden and Posidonia Shale in NW-Germany and the Netherlands: A 3D basin modelling study. Basin Research, 2016, 28(1): 2-33.

Chandra, D., Bakshi, T., Vishal, V. Thermal effect on pore characteristics of shale under inert and oxic environments: Insights on pore evolution. Microporous and Mesoporous Materials, 2021, 316: 110969.

Chen, S., Zhu, Y., Chen, S., et al. Hydrocarbon generation and shale gas accumulation in the Longmaxi Formation, Southern Sichuan Basin, China. Marine and Petroleum Geology, 2017, 86: 248-258.

Choudhury, T. R., Banerjee, S., Khanolkar, S. The geochemical affinity of paleogene glauconites in paleo-tethyan deposits of India, in Geochemical Treasures and Petrogenetic Processes, edited by J. S. Armstrong-Altrin, K. Pandarinath and S. K. Verma, Springer, Singapore, pp. 243-277, 2022.

Curtis, M. E., Cardott, B. J., Sondergeld, C. H., et al. Development of organic porosity in the Woodford Shale with increasing thermal maturity. International Journal of Coal Geology, 2012, 103: 26-31.

Dembicki, H. Three common source rock evaluation errors made by geologists during prospect or play appraisals. AAPG Bulletin, 2009, 93(3): 341-356.

Feng, Q., Qiu, N., Borjigin, T., et al. Tectonic evolution revealed by thermo-kinematic and its effect on shale gas preservation. Energy, 2022, 240: 122781.

Fu, Y., Jiang, Y., Wang, Z., et al. Non-connected pores of the Longmaxi shale in southern Sichuan Basin of China. Marine and Petroleum Geology, 2019, 110: 420-433.

Gao, Z., Fan, Y., Xuan, Q., et al. A review of shale pore structure evolution characteristics with increasing thermal maturities. Advances in Geo-Energy Research, 2020, 4(3): 247-259.

Guo, X., Li, Y., Borjigen, T., et al. Hydrocarbon generation and storage mechanisms of deep-water shelf shales of Ordovician Wufeng Formation-Silurian Longmaxi Formation in Sichuan Basin, China. Petroleum Exploration and Development, 2020, 47(1): 204-213.

Hazra, B., Dutta, S., Kumar, S. TOC calculation of organic matter rich sediments using Rock-Eval pyrolysis: Critical consideration and insights. International Journal of Coal Geology, 2017, 169: 106-115.

He, K., Zhang, S., Wang, X., et al. Effects of inorganic sulfur species on hydrocarbon conversion and 34S isotope fractionation during thermal maturation of Type II kerogen. Organic Geochemistry, 2022, 168: 104420.

Hickey, J. J., Henk, B. Lithofacies summary of the Mississippian Barnett Shale, Mitchell 2 T.P. Sims well, Wise County, Texas. AAPG Bulletin, 2007, 91(4): 437-443.

Jarvie, D. M., Hill, R. J., Ruble, T. E., et al. Unconventional shale-gas systems: The Mississippian Barnett Shale of north-central Texas as one model for thermogenic shale-gas assessment. AAPG Bulletin, 2007, 91(4): 475-499.

Jenkins, C. D., Boyer, C. M. Coalbed- and shale-gas reservoirs. Journal of Petroleum Technology, 2008, 60(2): 92-99.

Jin, Z., Nie, H., Liu, Q., et al. Source and seal coupling mechanism for shale gas enrichment in upper Ordovician Wufeng Formation-Lower Silurian Longmaxi Formation in Sichuan Basin and its periphery. Marine and Petroleum Geology, 2018, 97: 78-93.

Klaver, J., Desbois, G., Littke, R., et al. BIB-SEM pore characterization of mature and post mature Posidonia Shale samples from the Hils area, Germany. International

Journal of Coal Geology, 2016, 158: 78-89.

Li, Y. Mechanics and fracturing techniques of deep shale from the Sichuan Basin, SW China. Energy Geoscience, 2021, 2(1): 1-9.

Li, G., Gao, P., Xiao, X., et al. Lower cambrian organic-rich shales in Southern China: A review of gas-bearing property, pore structure, and their controlling factors. Geofluids, 2022a, 2022: 9745313.

Li, J., Li, H., Yang, C., et al. Geological characteristics and controlling factors of deep shale gas enrichment of the Wufeng-Longmaxi Formation in the Southern Sichuan Basin, China. Lithosphere, 2022b, 2022(Special 12): 4737801.

Liang, C., Jiang, Z., Zhang, C., et al. The shale characteristics and shale gas exploration prospects of the Lower Silurian Longmaxi shale, Sichuan Basin, South China. Journal of Natural Gas Science and Engineering, 2014, 21: 636-648.

Liu, S., Deng, B., Zhong, Y., et al. Unique geologic features of burial and superimposition of the Lower Paleozoic shale gas across the Sichuan basin and its periphery. Earth Science Frontiers, 2016, 23(1): 11-28. (in Chinese)

Liu, B., Mastalerz, M., Schieber, J. SEM petrography of dispersed organic matter in black shales: A review. Earth-Science Reviews, 2022, 224: 103874.

Liu, K., Ostadhassan, M. Multi-scale fractal analysis of pores in shale rocks. Journal of Applied Geophysics, 2017, 140: 1-10.

Liu, W., Wu, J., Jiang, H., et al. Cenozoic exhumation and shale-gas enrichment of the Wufeng-Longmaxi formation in the southern Sichuan basin, western China. Marine and Petroleum Geology, 2021, 125: 104865.

Makeen, Y. M., Abdullah, W. H., Pearson, M. J., et al. Thermal maturity history and petroleum generation modelling for the Lower Cretaceous Abu Gabra Formation in the Fula Sub-basin, Muglad Basin, Sudan. Marine and Petroleum Geology, 2016, 75: 310-324.

Nie, H., Li, D., Liu, G., et al. An overview of the geology and production of the Fuling shale gas field, Sichuan Basin, China. Energy Geoscience, 2020, 1(3-4): 147-164.

Peng, J., Pang, X., Shi, H., et al. Hydrocarbon generation and expulsion characteristics of Eocene source rocks in the Huilu area, northern Pearl River Mouth basin, South China Sea: Implications for tight oil potential. Marine and Petroleum Geology, 2016, 72: 463-487.

Peters, K. E., Xia, X., Pomerantz, A. E., et al. Chapter 3-geochemistry applied to evaluation of unconventional resources, in Unconventional Oil and Gas Resources Handbook, edited by Y. Z. Ma and S. A. Holditch, Gulf Professional Publishing, Boston, pp. 71-126, 2016.

Qiu, Z., Zou, C., Wang, H., et al. Discussion on the characteristics and controlling factors of differential enrichment of shale gas in the Wufeng-Longmaxi formations in south China. Journal of Natural Gas Geoscience, 2020, 5(3): 117-128.

Romero-Sarmiento, M. F., Ducros, M., Carpentier, B., et al. Quantitative evaluation of TOC, organic porosity and gas retention distribution in a gas shale play using petroleum system modeling: Application to the mississippian Barnett shale. Marine and Petroleum Geology, 2013, 45: 315-330.

Shalaby, M. R., Hakimi, M. H., Abdullah, W. H. Geochemical characteristics and hydrocarbon generation modeling of the Jurassic source rocks in the Shoushan Basin, north Western Desert, Egypt. Marine and Petroleum Geology, 2011, 28(9): 1611-1624.

Shi, X., Kang, S., Luo, C., et al. Shale gas exploration potential and reservoir conditions of the Longmaxi Formation in the Changning area, Sichuan Basin, SW China: Evidence from mud gas isotope logging. Journal of Asian Earth Sciences, 2022a, 233: 105239.

Shi, X., Luo, C., Cao, G., et al. Differences of main enrichment factors of S1l11-1 sublayer shale gas in Southern Sichuan Basin. Energies, 2021, 14(17): 5472.

Shi, Z., Zhou, T., Wang, H., et al. Depositional structures and their reservoir characteristics in the Wufeng-Longmaxi shale in Southern Sichuan Basin, China. Energies, 2022b, 15(5): 1618.

Tang, L., Song, Y., Jiang, S., et al. Sealing Mechanism of the roof and floor for the Wufeng-Longmaxi shale gas in the Southern Sichuan Basin. Energy & Fuels, 2020, 34(6): 6999-7018.

Wei, D., Zhao, Y., Liu, H., et al. Where will China's shale gas industry go? A scenario analysis of socio-technical transition. Energy Strategy Reviews, 2022, 44: 100990.

Xu, H., Zhou, W., Zhang, R., et al. Characterizations of pore, mineral and petrographic properties of marine shale using multiple techniques and their implications on gas storage capability for Sichuan Longmaxi gas shale field in China. Fuel, 2019, 241: 360-371.

Yang, R., He, S., Wang, X., et al. Paleo-ocean redox environments of the Upper Ordovician Wufeng and the first member in lower Silurian Longmaxi formations in the Jiaoshiba area, Sichuan Basin. Canadian Journal of Earth Sciences, 2016, 53(4): 426-440.

Zhang, K., Peng, J., Wang, X., et al. Effect of organic maturity on shale gas genesis and pores development: A case study on marine shale in the upper Yangtze region, South China. Open Geosciences, 2020, 12(1): 1617-1629.

Zhao, W., Zhang, B., Wang, X., et al. Differences in source kitchens for lacustrine in-source and out-of-source hydrocarbon accumulations. Petroleum Exploration and Development, 2021, 48(3): 541-554.

Zhu, C., Xu, M., Shan, J., et al. Quantifying the denudations of major tectonic events in Sichuan basin: Constrained by the paleothermal records. Geology in China, 2009, 36(6): 1268-1277.

Zou, C., Dong, D., Wang, Y., et al. Shale gas in China: Characteristics, challenges and prospects (I). Petroleum Exploration and Development, 2015, 42(6): 753-767.